# Effect of Bath Condition on the Diffusion of Contrast Agents Across Articular Cartilage

MASTER THESIS


Joaquin A. Villamar

November 19, 2014

*Department of Biomechanical Engineering – Tissue Biomechanics and Implants, Faculty of Mechanical, Maritime and Materials Engineering, Delft University of Technology (TU Delft)*

## General Information

| | |
|---|---|
| **Thesis Title:** | Effect of Bath Condition on the Diffusion of Contrast Agents Across Articular Cartilage |
| **Author:** | Joaquin Alberto Villamar |
| **Student Number:** | 4251946 |
| **E-mail Address:** | Joaquin.villamar@gmail.com |
| **Date:** | November 19, 2014 |
| **University:** | Delft University of Technology |
| **Master Program:** | MSc. Biomedical Engineering |
| **Course Code:** | BMA0332 |

## Graduation Committee:

Prof. Dr. Harrie Weinans
UMC Utrecht
TU Delft
H.H.Weinans@umcutrecht.nl

Dr. Ir. A. A. Zadpoor
TU Delft
A.A.Zadpoor@tudelft.nl

Dr. Liza Rassaei
TU Delft
l.rassaei@tudelft.nl

Behdad Pouran
UMC Utrecht
TU Delft
b.pouran@umcutrecht.nl

# Acknowledgments

I would like to thank my supervisors Dr. Ir. A. A. Zadpoor and Dr. H. H. Weinans, for their valuable and constructive suggestions during the preparation and execution of my research. A warm and special thanks goes to Behdad Pouran. During planning, data collection and writing we spent countless hours debating, brainstorming, proofreading and talking about my research. Your guidance made this a rewarding and thoughtful journey. I would also like to thank Vahid Arbabi for his contribution on the finite element simulation of this project and Nora Baka for her contribution, support and guidance on image registration process. You were both critical in my research.

I would like to acknowledge the Secretaria Nacional de Educacion Superior, Ciencia y Tecnologia (SENESCYT) for granting me with a scholarship to study in TU Delft. I extend my appreciation to the friendly staff at Utrecht Medical Center for their support.

Thank you to all my friends in Delft. Delihta, Hector, Ricard, Manuel, Andita, Lennart, Ricardo, Jose Miguel, Susana, Majka, Juan Camilo, you made this experience worthwhile. To my long time friends Edgar, Erick, Abel, Isil, Anna Laura, Mohammed, Josep, Walter thank you for your support and encouragement.

Last but not least, I thank my family: this thesis belongs to the Villamar Jorgge family. It is a combination of the knowledge dad gave me combined with the love and wonderful personality of mom. All I am today is because of both of you. Valeria, Xavier and Pancho this degree would not have been possible without any of you. I still remember how you all got together to help me come here. Your unequivocal support and love throughout, as always, for which my mere expression of thanks likewise does not suffice. To Wendy, your determination, support and courage got me back into my feet to keep moving forward, this degree is also for you.

Delft, November 2014

Joaquin Villamar

# Abstract

In the present study, the effect of concentration, osmolality and charge of x-ray contrast agents on their diffusion and equilibrium distribution across different zones of cartilage was investigated. Full-thickness cartilage discs (Ø = 8.5 mm, n = 3) were extracted from healthy equine femoral condyle (n = 2). The diffusion of four different contrast agent baths (Condition A: Visipaque 320 mg/ml, 290 mOsmol/kg; Condition B: Visipaque 320 mg/ml, 600 mOsmol/kg; Condition C: Visipaque 160 mg/ml, 290 mOsmol/kg; Condition D: Hexabrix 320 mg/ml, 600 mOsmol/kg) was allowed only through the articular surface. Samples were imaged with a micro computed tomography scanner (micro-CT) before the contrast agent bath was applied, and after 5, 10, 20, 30 minutes and 1, 2, 3, 4, 5, 6, 7, 10, 12, 24, 30, 36, and 48 hours. Findings show that osmolality and concentration do not have a pronounced effect on diffusion. However, concentration influence on diffusion is seen on zonal curves. Moreover, the diffusion coefficient of Hexabrix was between 2.9 and 8.6 times lower than that of Visipaque that reflects the important effect of solute's charge on the transport through charged hydrated tissue such as articular cartilage. Slightly different diffusion coefficient observed within dilute and concentrated Visipaque baths suggested deviation from ideal Fickean behavior within articular cartilage. However, close diffusion coefficients of cartilage exposed to low and high osmolality baths confirmed the minor effect of osmolality on the transport of neutral solutes.



**Keywords:** articular cartilage; diffusion; contrast agent; contrast enhanced computed tomography (micro-CT); Visipaque; Hexabrix; cartilage zones; diffusion coefficient

## TABLE OF CONTENTS

# 1. Introduction

Articular cartilage is an avascular, structurally organized, smooth and flexible connective tissue found between gliding joints. It allows mobility between articulating surfaces with minimal friction and wear while distributing joint loads to decrease joint surfaces' stresses [1]. Articular cartilage is made of a solid matrix and a fluid phase. Collagen and glycosaminoglycans (GAGs) are the main components of the solid matrix of articular cartilage whereas water and mobile ions are the main components of the fluid phase. GAGs are negatively charged polysaccharides covalently attached to proteoglycans in the extracellular matrix (ECM) and they are responsible of holding water in the tissue and allowing cartilage to resist compression [2, 3].

Articular cartilage comprises of different layers with inhomogeneous collages as well as GAG distribution. Figure 1 [4] illustrates the structure of cartilage zones. These zones are categorized into superficial, middle, deep and calcified zones. Superficial zone is made of fine fibers that are densely packed parallel to the articular surface; it has a high cell density and a low GAG content in comparison to the other zones. In the middle zone has thicker collagen fibers in comparison to the superficial zone and they are randomly oriented. Also, the middle zone has the highest concentration of GAGs. In the deep zone, the fibers reach their maximal thickness and orient perpendicularly to the articular surface and form bundles [5] that cross the tidemark in the calcified zone and fixes the articular cartilage to the bone [6]. Water content in cartilage reduces linearly with depth going from 80% in the superficial zone to 65% in the deep zone [7]

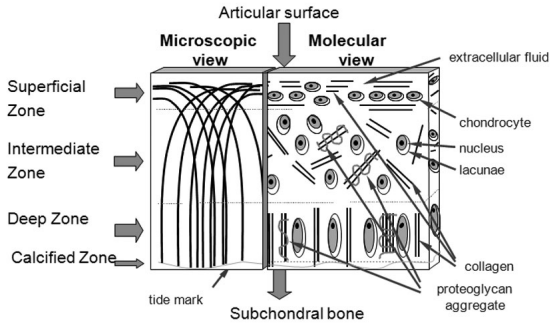


**Figure 1 –** Illustration of the cartilage microstructure with the different zones, macromolecules and fiber orientations present in cartilage [4].

As an avascular tissue, cartilage health relies on diffusion and convection for the transport of nutrients and small molecules between cartilage and the surrounding synovial fluid [1]. Moreover, water has free mobile cations that can alter the physicochemical and mechanical properties of cartilage [8, 9] giving cartilage its load bearing capability. The main mechanism for the transport of ions and macromolecules are diffusion and convection, respectively [10]. Diffusion is a mechanism of mass transport that occurs due to random particle motion leading eventually to a homogeneous mix. Convection however, is the transport of matter due to the motion of fluid as a result of body forces [11].

Fick's laws and Brownian motion are the corner stones of diffusion [12]. Brownian motion is responsible for the particles' random movements. But, if a chemical potential is present, particles will tend to move from a high chemical potential area to a low chemical potential area. This is known as Fick's first law and in one dimension this law is expressed as follows [12]

$$J = -D\frac{\partial C}{\partial x} \tag{1}$$

where $J$ is the diffusion flux (mol/m$^2$.s), $D$ is the diffusion coefficient and $\frac{\partial C}{\partial x}$ is the concentration gradient. The microstructural features, temperature of the environment as well as size of the diffusing molecules influence the diffusion coefficient, which is an inherent property of the medium [13]. Due to its sensitivity on the local microstructure, diffusion coefficients are used in current studies to assess the physical properties of tissues like cartilage [14-16]. In particular situations, diffusion can also be recognized as a non-Fickean process. Unlike Fickean diffusion, non-Fickean diffusion is concentration-dependent. An example of non-Fickean diffusion can be found when an ionic solvent diffuses in articular cartilage that results in matrix deformation. This geometrical change during diffusion may alter ion-extracellular matrix (ECM) interactions due to water content as well as steric hindrance changes [17-19]. Consequently, the diffusion process undergoes temporal changes resulting in deviation from simple Fickean assumption.

The function of cartilage is compromised when the main components are disturbed affecting the interaction between them. The progressive degeneration of articular

cartilage and subchondral bone that causes cartilage's mechanical property deterioration is called osteoarthritis (OA). The initial signs of OA are disruption of collagen network, GAG depletion, alteration of water content and thickening of subchondral bone [3, 20-23]. These disruptions cause an alteration of the diffusive properties of cartilage [24] which can be used by imaging techniques as a marker to evaluate cartilage integrity [16]. Contrast enhanced computed tomography (CECT) quantifies GAG concentration in cartilage by imaging diffusion and equilibrium partitioning of a contrast agent using a CT scanner. The contrast agents used in CECT can have a positive, negative or neutral charge [25] and their diffusion rate and equilibration varies accordingly. For an anionic contrast agent, the diffusion rate and equilibrium partitioning is inversely proportional to the negatively charged GAG concentration [9]. The opposite is expected for a cationic contrast agent is used [26]. In the case of a contrast agent with no charge, GAG concentration does not affect its diffusion. Other constituents like molecular weight of the contrast agent, the direction of the collagen network and water content enhance the complexity of contrast agent diffusion [14, 27-31]. Moreover, salts are added to contrast agent baths to reach a particular osmolality to emulate the osmolality of a normal synovial fluid. Salts are composed of ions, which may influence the contrast agent diffusion. This has not been studied before.

The aims of this thesis are to use three intact osteochondral plugs to: (1) determine the effect of concentration of the uncharged contrast agent Visipaque on diffusion; (2) determine if osmolality has an effect on the diffusion process of Visipaque; (3) compare the diffusion of the negatively charged contrast agent Hexabrix against the uncharged contrast agent Visipaque; (4) addressing the diffusion in the different zones of cartilage for different conditions.

# 2. Methodology

The research questions for this study were: (1) the effect of concentration of the uncharged contrast agent Visipaque on diffusion; (2) the effect of osmolality on the diffusion process of Visipaque; (3) comparison of the diffusion of the negatively charged contrast agent Hexabrix against the uncharged contrast agent Visipaque; (4) analysis of the zonal diffusion in cartilage of four different contrast agent baths. To address these questions an experimental setup was designed as shown on figure 2.

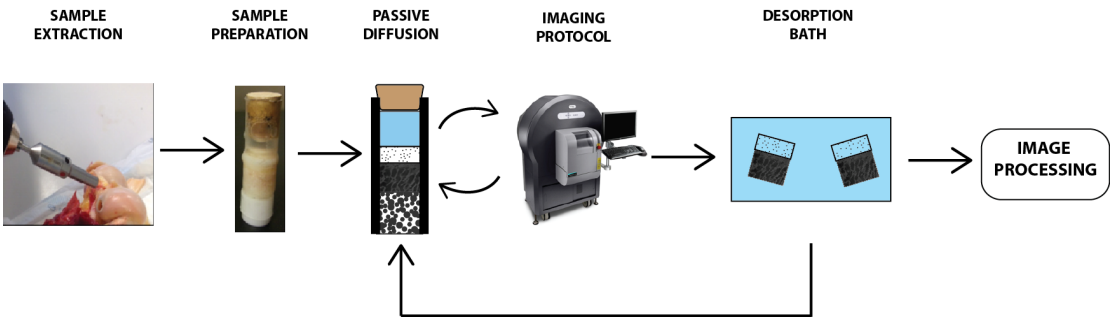


**Figure 2 –** Flow chart of the experimental setup.

## 2.1. Sample Preparation

### 2.1.1. Sample Extraction and Conditioning

For this study, equine knees were obtained from the Equine Clinic in Utrecht University. Using a drill driver, three osteochondral plugs were harvested non-sterilely from visually intact medial femoral condyle of 6-10 year-old euthanized equine donors immediately after the animals were sacrificed. To reduce the effects of spatial variations in cartilage properties, osteochondral plugs were extracted as close to each other as possible. The Utrecht University Animal Experiments Committee approved the procedures. The harvesting involved drilling the joints with a custom-made drill tips (ACUFEX, Smith-Nephew, USA) associated with continuous drill site irrigation using PBS to prevent overheating. To avoid damaging the cartilage during extraction, the drill tip had to be pressed perpendicular to the cartilage surface prior to the drilling as shown on figure 3(a). The surface was checked visually to detect

potential damages made by the drill. The average height of the explants was 12.5 ± 2.5 mm and the diameter was 8.5 mm shown on figure 3(b). Cartilage's thickness was 2.9 ± 0.2 mm. Osteochondral plugs were subsequently transferred to vials containing PBS with a pH of 7.4, one tablet of protease inhibitor and 0.36 mg of EDTA per ml of solution to prevent cartilage degradation. Moreover, the osmolality of the solution was adjusted to 290 mOsmol/kg to match the osmolality of the synovial fluid in the horse joint. The specimens were then stored in the freezer at -20 ºC prior to the preparation of the tissue sample.

### 2.1.2 Tissue Sample Preparation

The preparation of the samples started by thawing the frozen osteochondral plugs at 4 ºC for five hours. Once the samples were completely defrosted, they were wrapped in a heat shrinkable tube in combination with hot melt adhesive (SBRS-3XGLW, Woer, China) as shown on figure 3(c) The wrapping procedure was intended to minimize edge effects as well as radial diffusion from the sides of the sample. On the upper part of the sample a cork plug was placed to restrict the evaporation of the contrast agents during prolonged diffusion experiments. In addition, a POM support was mounted underneath the osteochondral plug for specimen stabilization in the micro-CT scan.

(a) (b) (c)

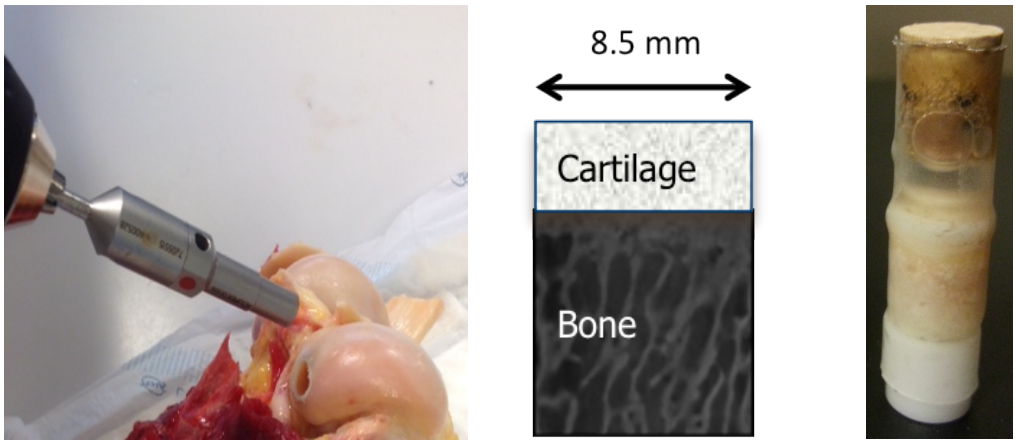


**Figure 3 –** (a) The drill tip had to be pressed perpendicularly to the cartilage surface prior to the drilling procedure to avoid damaging the cartilage during extraction. (b) The diameter of the osteochondral plug was 8.5 mm and the average height of the

explants was 12.5 ± 2.5 mm. (c) The tissue sample is composed of a cork on the upper part. Below the cork is the contrast agent followed by the cartilage and finally the support. All components are wrapped with a heat shrinking tube.

## 2.2 Solute Transport

This thesis assessed the transport of two different contrast agents in horse articular cartilage at different concentrations and at different osmolalities resulting in four different conditions summarized in table 2.1. For condition C, the contrast agent is diluted using distilled water to reach a concentration of 160 mgIodine/ml. For conditions A, B and D the original concentrations of the contrast agents was used. Conditions A, C and D used contrast agents with unaltered osmolality. For condition B, the osmolality of the contrast agent was increased to 600 mOsmol/kg by adding 0.3 gr NaCl/ml. The osmolalities for conditions A to D were measured with a micro-osmometer (3320, Advanced Instruments, USA).

**Table 2.1:** Summary of concentrations and osmolalities used in conditions A to D.

| Condition | Contrast Agent | Concentration [mgIodine/ml] | Osmolality [mOsmol/kg] |
|---|---|---|---|
| **A** | Visipaque™ | 320 | 290 |
| **B** | Visipaque™ | 320 | 600 |
| **C** | Visipaque™ | 160 | 290 |
| **D** | Hexabrix™ | 320 | 600 |

For conditions A to D, 600-700 µL of contrast agent were injected over the articular surface in the osteochondral plug. Immediately, the cork was placed on top of the sample to avoid the evaporation of the contrast agent after prolonged diffusion experiments. The study was conducted at room temperature (20 ºC). Table 2.2 summarizes the characteristics of contrast agents used in conditions A to D.

**Table 2.2:** Summary of characteristics of the contrast agents used in conditions A to D.

| Contrast Agent | Active Moiety | Charge | Molecular Mass [g/mol] | Manufacturer |
|---|---|---|---|---|
| Visipaque™ | Iodixanol | 0 | 1550 | GE Healthcare AS, Netherlands |
| Hexabrix™ | Ioxaglate | -1 | 1269 | Mallinckrodt, St. Louis, MO, USA |

## 2.3 Imaging Protocol

A micro-CT scanner (Quantum FX, Perkin Elmer, USA) was used to investigate diffusion for conditions A to D and is shown in figure 4(a) The micro CT-scanner was set to a tube voltage of 90 kV, tube current of 180 mA and voxel size of 40 $\mu m^3$. Initially, the osteochondral plugs were mounted over a custom-made support, placed inside the micro-CT chamber and imaged without contrast agent. Afterwards, 600-700 µL of contrast agent (Table 2.2) was injected in the free space in the wrapping above the articular cartilage and the diffusion progress was recorded in 0, 5, 10, 20, 30 minutes and 1, 2, 3, 4, 5, 6, 7, 10, 12, 24, 30, 36 and 48 hours. Samples were mounted on a custom holder as shown on figure 4(b). Samples 1 and 2 were imaged simultaneously while sample 3 was imaged by itself. A total of three samples were imaged per condition.

(a) (b)

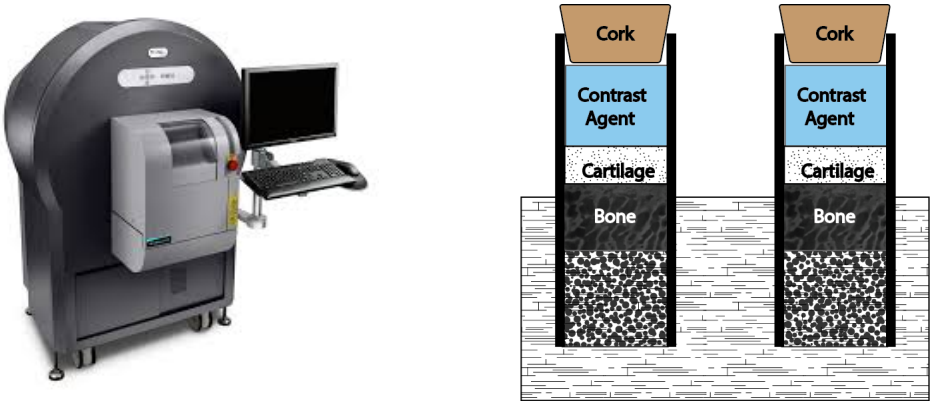


**Figure 4 –** (a) Micro-CT Scanner used for image acquisition model Quantum FX Perkin Elmer. Tube voltage: 90 kV, tube current: 180 mA, resolution: 40 µm. (b) Two prepared tissue samples were mounted on a custom made holder and imaged simultaneously.

## 2.4 Desorption Bath

After 48 hours, when the contrast agent reached equilibrium in the cartilage, the wrapping material around the sample was removed. The samples were put into a rinsing solution of 50 ml made of PBS, EDTA and protease inhibitor for 24 hours at a temperature of 5 °C. After 24 hours, the samples were removed from the rinsing solution and were placed in a new rinsing solution of 50 ml with the same characteristics for another period of 24 hours. This procedure was done to reutilize the tissue samples for conditions A to D.

## 2.5 Image Processing

### 2.5.1 Equilibrium Curves

Equilibrium curves were generated using the average grey values obtained by using the public domain ImageJ program developed at the US National Institutes of Health [32]. The micro-CT scanner generated tomographic grayscale images of three osteochondral plugs for each condition. The mid-section of the tomographic grayscale

image was selected for each sample. Then a region of interest (ROI) was generated and used to crop the original image. All ROIs for the same sample at a specific condition had to be the same. That is, they had to be located in the same coordinates and they had to have the same width. All samples in conditions A to D had ROI's of the same width, 140 pixels. The height did vary between conditions and samples. All ROIs included three sections: contrast agent, cartilage and subchondral bone. The following step was thresholding that led to the generation of a mask of the cartilage thickness at each time point. To segment cartilage, two global threshold values were used: one to segment subchondral bone and the other to segment the contrast agent above the cartilage. The ROIs of both segmentations were added and the resulting image was inverted. This resulted in a mask of the cartilage section. BoneJ, and ImageJ plug-in that uses a greater sphere-fitting algorithm [33], used the mask to calculate the average cartilage thickness. The final step was obtaining the average grey value of the full cartilage. The contours of the masks of the cartilage section of the osteochondral plugs at all time points were selected using the wand tool in ImageJ and stored in the ROI manager. The original grey scale ROIs were opened and the corresponding contours were selected from the ROI manager to measure the average grey values. The average grey values were converted by the following linear relationship formula

$$C = H * \alpha + \beta \tag{2}$$

Where $C$ is the contrast agent bath concentration, $H$ is the average grey value of cartilage and $\alpha$ and $\beta$ are constants. To find $\alpha$ and $\beta$, two equations were generated. The highest concentration is related to the highest average grey value to form one equation. Relating the lowest concentration to the lowest average grey value generated a second equation. The final step was normalizing the concentration and it was achieved by dividing the concentration by the original bath concentration of the corresponding condition and the result was multiplied by one hundred. These values are plotted with respect to time. Figure 5 illustrates the steps previously described to obtain the average grey values.


**Figure 5 –** Flowchart of image processing with ImageJ for the generation of the equilibrium curves.

### 2.5.2 Image Registration

A rigid registration process was performed with the Elastix software [34]. Two images are required to perform the registration process, a moving image $I_M(x)$ and a fixed image $I_F(x)$. Images at time 0 minutes for conditions A to D and for samples 1 to 4 were selected as fixed images. Images at times 12, 24, 30 and 48 hours for conditions A to D and for samples 1 to 4 were selected as moving images. Registration was performed between fixed and moving images from the same condition and same sample number. Registration is the task of finding the transformation $T(x) = x + u\ (x)$ that spatially aligns $I_M(T(x))$ to $I_F(x)$. The quality of the alignment is determined by the cost function $C\ (\boldsymbol{T}\colon I_F, I_M)$ also known as metric. Registration is mathematically formulated as an optimization problem in which $C$ is reduced to its minimum with respect to $T$ to achieve the optimal transformation. Elastix software limits the amount of possible transformations by introducing a parameterization of the transformation. The optimization problem is expressed as [34]

$$\hat{\mu} = \arg\min_{\mu} C(T_\mu\,; I_F, I_M) \tag{3}$$

where the subscript μ denotes the parameterization of the transform. The transformation parameters are contained on vector μ. The minimization of the cost function $C$ is achieved through an iterative optimization method, frequently in a multi-resolution setting. Figure 6 illustrates the basic registration components used by the Elastix software and which can be configured to create a registration algorithm.

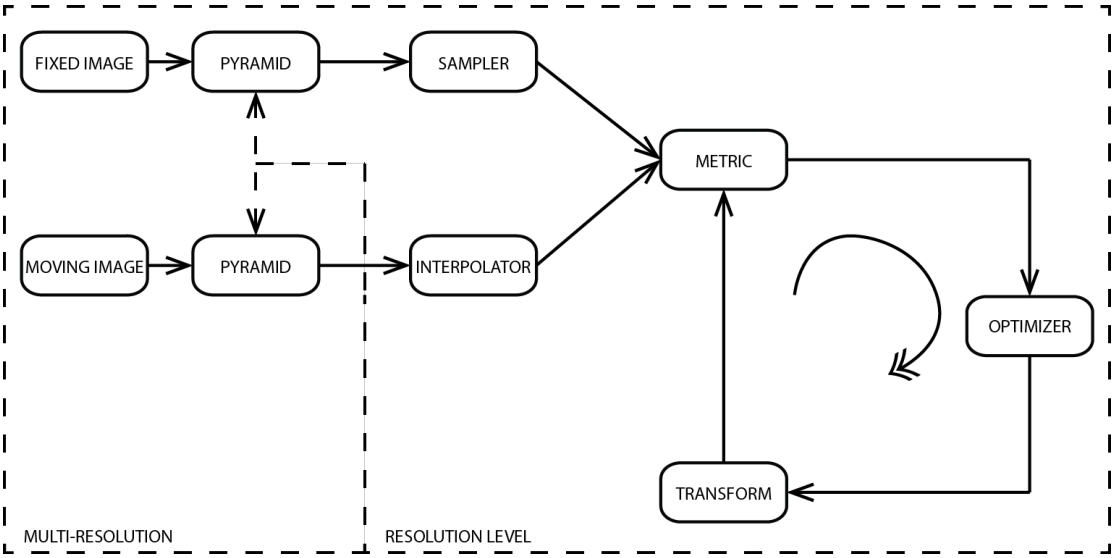


**Figure 6 –** Flowchart of basic registration components [34].

Registration was optimized using 1024 iterations using Mutual Information (MI) as the cost function. MI was calculated using 2048 samples per iteration from a sample region of size 50 x 50 x 50 mm. MI measures the statistical dependence between the intensities of the fixed and moving images [35] and is defined as follows [36]

$$MI(\mu; I_F, I_M) = \sum_{m \in L_M} \sum_{f \in L_F} p(f, m, ; \mu) log_2 \left( \frac{p(f, m; \mu)}{p_F(f) p_M(m; \mu)} \right) \quad (4)$$

where $L_F$ and $L_M$ are sets of intensity bin centers that are regularly spaced, the discrete joint probability is represented by $p$. The marginal discrete probabilities of the moving and fixed images are represented by $p_m$ and $p_F$.

A linear interpolator was used when applying the deformation to the moving image. The values obtained with the linear interpolator are the weighted average of the neighboring voxels and the weight is the distance to each voxel. A translation transformation was called in the algorithm and is defined as [34]

$$T_\mu(x) = x + t \quad (5)$$

where $t$ is the translation vector. The exact registration settings can be found on the appendix A and a usage example of Elastix can be found on appendix B. The parameter vector is defined by $\mu = t$. Elastix is a command-line program with no

graphical user interface. Thus, MeVisLab was used as a visualization tool used to compare the fixed image to the registered image [37]. Using Panel Synchroview for 2D, random points in the cartilage surface and in the boundary between the cartilage and the subchondral bone were selected to visually inspect if the points in the fixed and the registered image matched as shown in figure 7.

a) b)

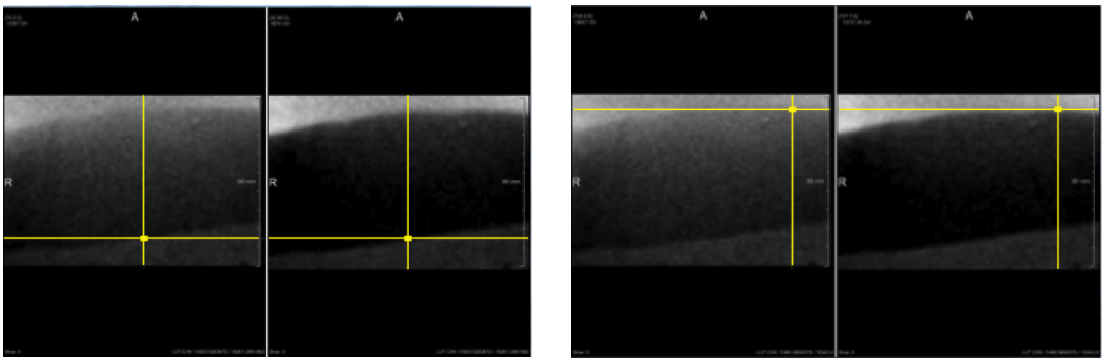

**Figure 7 –** Visual inspection of the registered image using MeVislab. Random points in the (a) boundary between the cartilage and the subchondral bone and the (b) cartilage surface were selected to visually inspect if the points in the fixed and the registered image matched.

### 2.5.3 Concentration Gradient Curves

Images registered with ImageJ required post-processing with ImageJ. After registration, the images may have pixels that come from outside the picture. This occurs when there is no correspondence between some pixels at time t = 0 hours and t > 0 hours. In this thesis, this was the case for all registered images at their borders. To identify these pixels in the registered image, in the Elastix parameter file a default pixel value of 0 was set. Using ImageJ, the identified pixels were cropped from the registered image. The mask previously created for t = 0 hours for the same sample and condition as the registered image, was cropped to the same size and at the same coordinates as the registered image. The resulting mask was used to generate multiple ROIs of a one-pixel thickness and applied on the registered image to obtain the average grey values for each ROI at different depths in cartilage. The average grey

values were converted into concentration using the $\alpha$ and $\beta$ values previously obtained for each condition for the equilibrium curves in combination with equation (2). The normalized concentrations were obtained by dividing the concentration by the original bath concentration of the corresponding condition and the result was multiplied by one hundred. To normalize thickness, a particular ROI had to be divided by the total number of ROIs that cover a sample's thickness. Figure 8 summarizes the steps previously described to obtain the concentration gradient curves.


**Figure 8 -** Flowchart of image processing with ImageJ and Elastix to generate the concentration gradient curves.

### 2.5.4 Zonal Diffusion Curves

Zonal diffusion curves were generated based on the previously registered images at 0, 1, 6, 12, 24 and 48 hours for conditions A to D and samples 1 to 3. The first step was to determine the thickness of cartilage at 0 hours for each sample using BoneJ plug-in in ImageJ [33]. Then, for each image, cartilage was divided in three zones: superficial, middle and deep zones. The superficial zone is equivalent to 20% of cartilage thickness from the surface. The next 50% of cartilage's thickness from the end of the superficial zone was considered middle zone and the final 30% of cartilage's thickness at the end of the middle zone was considered the deep zone. The multiple ROIs previously generated for the concentration gradient curves were then used. The multiple ROIs of one pixel thickness were combined to cover the superficial, middle and deep zones separately by using the OR option in ImageJ creating three new ROIs, one for each zone. These ROIs were applied to the registered images at 0, 1, 6, 12, 24 and 48 hours for conditions A to D and samples 1 to 3 and the average grey values were obtained. The average grey values were converted into concentration using the $\alpha$ and $\beta$ values previously obtained for each condition for the equilibrium curves in combination with equation (2). The normalized concentrations were obtained by dividing the concentration by the original

bath concentration of the corresponding condition and the result was multiplied by one hundred.

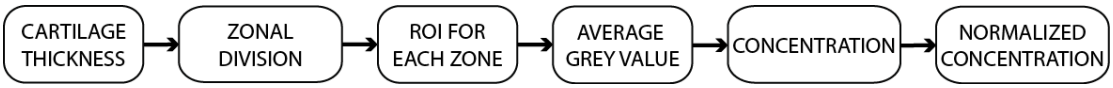


**Figure 9 –** Flowchart of ImageJ and Elastix to generate the zonal diffusion curves

## 2.6 Diffusion Coefficient

For this thesis, it was assumed that the cartilage disks were exposed to a stirred solution with limited volume. Thus, the concentration in the solution depends on time and is determined by the condition that the total amount of solute in the cartilage and in the solution remains constant as diffusion progresses. Moreover, the thickness of cartilage was assumed to be $2l$ and that diffusion occurred in one dimension only through the articular cartilage. The solution, of limited size, occupies the space $-l-a \leq x \leq -l$, $l \leq x \leq l+a$. Furthermore, the solute's concentration in the solution is initially $C_0$ and is permanently uniform. Cartilage is initially free from the solute.

A solution for the diffusion equation is required [17]

$$\frac{\partial C}{\partial t} = D\frac{\partial^2 C}{\partial x^2} \tag{6}$$

with the following initial condition

$$C = 0, \qquad -l < x < l, \qquad t = 0 \tag{7}$$

Another boundary condition is based on conservation of mass at the cartilage-bath interface stating that the rate at which a solute enters the cartilage over the surface $x = l$ is the same at which it leaves the solution. This boundary condition is expressed as follows

$$a\frac{\partial C}{\partial t} = \pm \mathrm{D}\frac{\partial C}{\partial x}, \qquad x = l, \qquad t > 0 \tag{8}$$

The concentration within the cartilage is given by the expression [38]

$$C = C_{\infty}\left\{1 + \sum_{n=1}^{\infty} \frac{2(1+\alpha)\exp\left(-\frac{Dq_n^2 t}{l^2}\right)}{(1+\alpha+\alpha^2 q_n^2)} \frac{cos\left(\frac{q_n x}{l}\right)}{cos q_n}\right\} \tag{9}$$

where $q_n$ are the non-zero positive roots of

$$\tan q_n = -\alpha q_n \tag{10}$$

and

$$\alpha = \frac{a}{kl} \tag{11}$$

where $a$ is the bath height, $l$ the cartilage height and $k$ the partition factor calculated by dividing the average grey value at 48 hours over the average grey value of the solution. FEBio software was used to develop a one dimensional finite element model to fit the experimental data for all conditions in the equilibrium curves to obtain the diffusion coefficients [39].

### 2.6.1 Statistical Analysis

ANOVA two-factor without replication statistical analysis was used to determine the statistical significance of the normalized concentrations at 48 hours in the equilibrium curves as well as in the zonal curves.

# 3. Results

To highlight the effect of contrast agent's concentration, osmolality and charge in its passive diffusion through cartilage the equilibrium curves, zonal equilibrium curves and concentration gradient curves were generated for each sample at different conditions. For the equilibrium curves, the normalized concentration of the full cartilage for conditions A through D were plotted as a function of time as shown in figure 10a, 10b and 10c. By comparing the equilibrium curves of conditions A and C the effect of concentration variation of Visipaque on diffusion was observed. In figures 10a, 10b and 10c, conditions A and C reached near equilibrium state at 24 hours. The normalized concentrations for both conditions were close for all samples. However, on average condition C had a higher rate of diffusion up to time 10 hours in comparison to condition A. The effect of osmolality on diffusion was assessed by comparing the equilibrium curves of conditions A and B that represent Visipaque diffusion at different osmolalities but with the same concentration. For both conditions the near equilibrium state was reached at 24 hours as shown on figure 10a, 10b and 10c. On average the diffusion rate of both conditions were similar as well as the normalized concentrations for all different time points. Comparing conditions B and D in the equilibrium curves assessed the effect of charge on diffusion. Condition B was composed of Visipaque, a contrast agent with neutral charge and Condition D was composed of Hexabrix, a contrast agent with a negative charge. Both conditions had the same osmolality and both contrast agents have similar molecular size. For both conditions the near equilibrium state was reached at 24 hours as shown in figure 10a, 10b and 10c. Moreover, condition B had a higher diffusion rate from 0 hours until 10 hours as well as a higher normalized concentration at all time points. The normalized concentration at the near equilibrium state for conditions A, B, C and D were 27.8 ± 4.6 % (mean ± SD), 28.1 ± 8.8 %, 30.9 ± 7.1 % and 12.1 ± 1.4% respectively. The partition coefficients, equivalent to the normalized concentrations at 48 hours, of the equilibrium curves are shown on table 3.1. The difference between partition coefficients of condition B and D was statistically significant ($P < 0.05$).

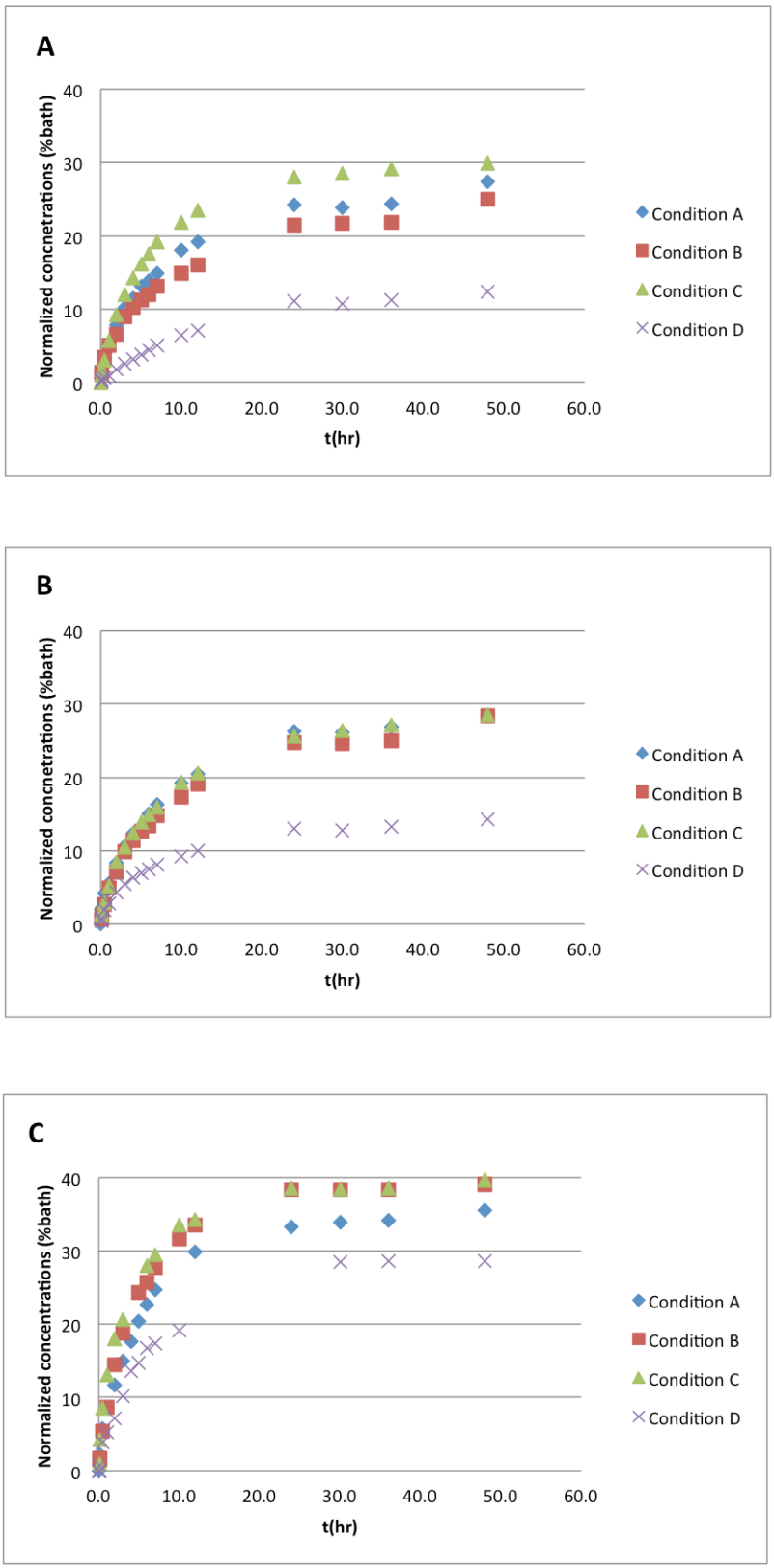


**Figure 10 –** Normalized concentrations in full thickness cartilage at different time points for (a) sample 1, (b) sample 2 and (c) sample 3 for conditions A through D.

**Table 3.1 –** Partition coefficients (normalized concentrations at 48 hours) for the equilibrium curves. Only conditions B and D had a statistically significant difference ($P < 0.05$).

| A | B | *P-value* | A | C | *P-value* | B | D | *P-value* |
|---|---|---|---|---|---|---|---|---|
| 33.7 ± 5.9 | 30.7 ± 7.4 | 0.8399 | 33.7 ± 5.9 | 33.0 ± 6.1 | 0.0942 | 30.7 ± 7.4 | 18.3 ± 9.3 | 0.0094 |

The zonal curves provided more details about contrast agent diffusion in three different zones in cartilage: superficial, middle and deep zones. Figure 11 illustrates the normalized concentration of sample 1 and condition B in the superficial, middle and deep zones of cartilage at different time points. Figure 12 shows the normalized concentration against time of conditions A-D for samples 1 and 2 in the three different zones of cartilage. The normalized concentrations for the superficial zone were higher, for all samples and conditions, than those in the middle and deep zones as shown in figures 11 and 12. In the superficial zone for all conditions, the highest diffusion rate occurred in the interval of time between 0 and 1 hour as shown in figure 12. Condition C had the highest rate of diffusion. Conditions A and B had a similar rate of diffusion, slower than condition C but higher than the diffusion rate of condition D. All conditions reached near-equilibrium normalized concentrations at approximately 12 hours in the superficial zone. In the superficial zone at 48 hours, condition B and D reached the highest and lowest partition coefficients respectively. The normalized concentrations at near equilibrium state for conditions A, B, C and D in the superficial zone were 57.7 ± 1.8 %, 59.3 ± 8.6 %, 53.4 ± 6.8 % and 29.7 ± 1.0 % respectively. In addition, the partition coefficients for conditions A, B, C and D in the superficial zone were 57.7 ± 1.8 %, 59.3 ± 8.6 %, 53.4 ± 6.8 % and 29.7 ± 1.0 % respectively. In the middle zone, condition C starts diffusing immediately after time 0 hours as shown in figure 12. Conditions A, B and D start diffusing in the middle zone after time 1 hour. The highest rate of diffusion in the middle zone occurs for all conditions and samples in the time interval 1 to 6 hours. Condition C and A have the highest rate of diffusion followed by condition B and lastly condition D. In the middle zone, no condition reaches equilibrium after 48 hours. Condition C and condition D reached the highest and lowest partition coefficients at time 48 hours respectively. The partition coefficients for conditions A, B, C and D in the middle zone were 30.1 ± 5.0 %, 28.7 ± 5.6 %, 33.7 ± 6.7 % and 13.4 ± 0.2 respectively. In the deep zone,

diffusion starts after time 6 hours for conditions A and C and after time 12 hours for conditions B and D as shown in figure 12. Also, condition C has the highest diffusion rate of all conditions and it is highest between 6 and 24 hours. The diffusion rate of conditions A and B are similar and their highest diffusion rate was occurred between 12 and 24 hours. The lowest diffusion rate is that of condition D and it is fastest between 12 and 24 hours. In the deep zone condition C and condition D reached the highest and lowest partition coefficients respectively. In the deep zone, no condition reaches equilibrium after 48 hours. The partition coefficients for conditions A, B, C and D in the deep zone were 16.5 ± 3.8 %, 16.0 ± 2.6 %, 20.2 ± 4.1 % and 5.8 ± 1.6 % respectively. A summary of the partition coefficients for all zones and conditions is listed on table 3.2. The difference between partition coefficients of condition B and D in all cartilage zones was statistically significant ($P < 0.05$) as well as the difference between A and C in the deep zone ($P < 0.05$).

**Table 3.2 –** Summary of partition coefficients for conditions A-D in the superficial, middle and deep zones of cartilage as well as their statistical significance.

**Superficial**

| A | B | *P-value* | A | C | *P-value* | B | D | *P-value* |
|---|---|---|---|---|---|---|---|---|
| 57.7 ± 1.8 | 59.3 ± 8.6 | 0.7551 | 57.7 ± 1.8 | 53.4 ± 6.8 | 0.4010 | 59.3 ± 8.6 | 29.7 ± 1.0 | 0.0242 |

**Middle**

| A | B | *P-value* | A | C | *P-value* | B | D | *P-value* |
|---|---|---|---|---|---|---|---|---|
| 30.1 ± 5.0 | 28.7 ± 5.6 | 0.1296 | 30.1 ± 5.0 | 33.7 ± 6.7 | 0.2668 | 28.7 ± 5.6 | 13.4 ± 0.2 | 0.0430 |

**Deep**

| A | B | *P-value* | A | C | *P-value* | B | D | *P-value* |
|---|---|---|---|---|---|---|---|---|
| 16.5 ± 3.8 | 16.0 ± 2.6 | 0.4227 | 16.5 ± 3.8 | 20.2 ± 4.1 | 0.0082 | 16.0 ± 2.6 | 5.8 ± 1.6 | 0.0474 |

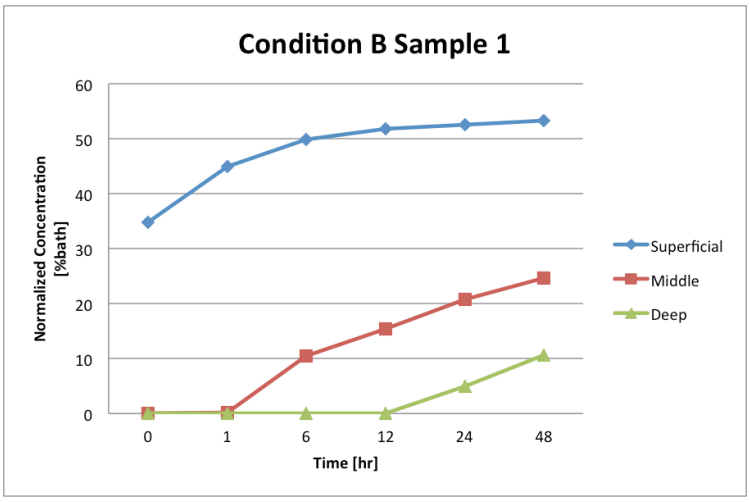


**Figure 11 –** Zonal curves for condition B sample 1. The concentration of the contrast agent versus time is illustrated at different time points in different zones.

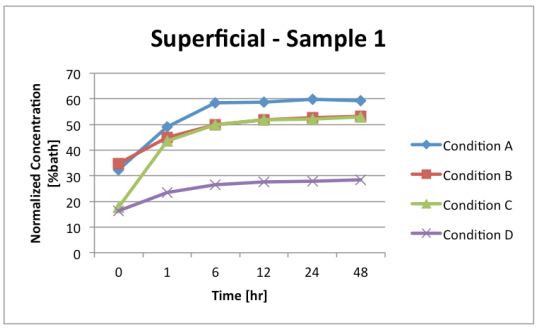


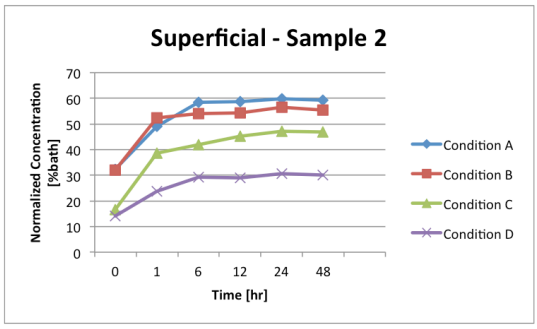


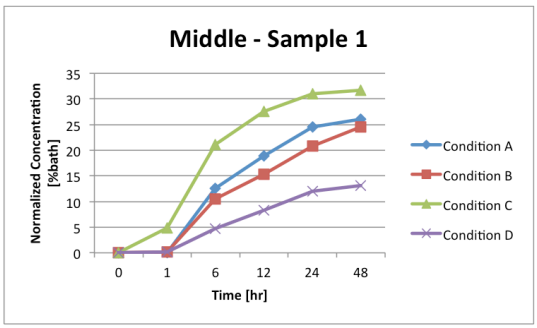


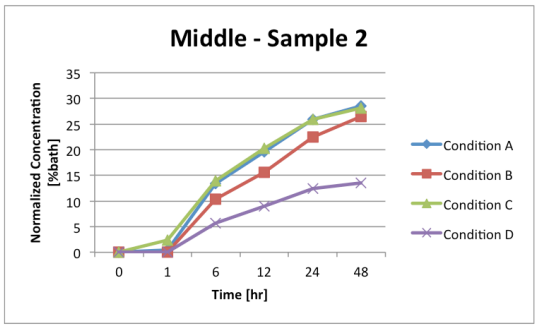


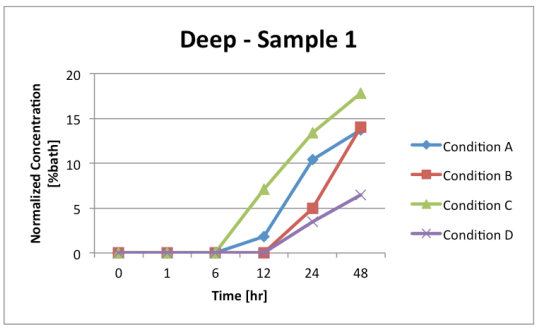


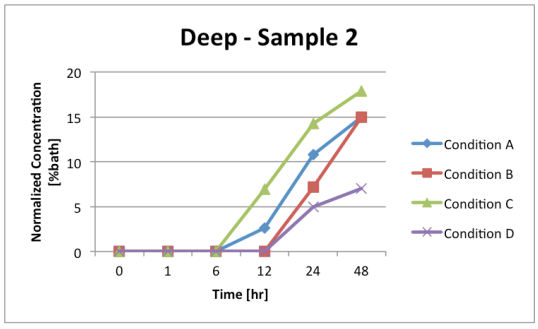

**Figure 12 –** Equilibrium curves for the superficial, middle and deep layers of cartilage for samples 1 and 2. These curves are called in this study zonal equilibrium curves.

For the concentration gradient curves, the normalized concentration of multiple one-pixel thickness ROIs were plotted against depth as shown on figure 13. The superficial zone is equivalent to 20% of cartilage thickness from the surface. In the superficial zone, condition A had the highest rate of diffusion followed by conditions B and C that had similar normalized concentrations as well as rate of diffusion. Condition D that had the lowest normalized concentration and rate of diffusion in the superficial zone. The middle zone corresponds to the next 50% of cartilage's thickness after the end of the superficial zone. In the middle zone, the diffusion rate and normalized concentration diminishes for all conditions. In this zone, condition C has the highest diffusion rate, followed by conditions A and B and finally condition D. The deep zone is equivalent to the final 30% of cartilage's thickness at the end of the middle zone. In the deep zone the diffusion rate as well as the normalized concentrations lower for all conditions. Condition C had the highest normalized concentration followed by conditions A and B. Condition D had the lowest normalized concentration in the deep zone. The partition coefficients for conditions A, B, C and D at 86% of the total cartilage thickness from the surface are 10.4 ± 1.7 %, 7.4 ± 2.7 %, 17.8 ± 2.6 % and 6.2 ± 1.3 % respectively.

Using a one dimensional finite element model developed with FEBio software the diffusion coefficients for all conditions and samples were calculated. This model fitted the computational values to the experimental data based on the superficial zone. The experimental data was obtained from the equilibrium curves. A summary of the diffusion coefficients is listed in table 3.3.

Table 3.3 illustrates that osmolality alteration only slightly affects the diffusion coefficient within the articular cartilage (comparison between A and B). The ratio of diffusion coefficients for condition A and condition B ($D_A/D_B$) and for samples 1 to 3 is 1.38, 1.23 and 0.76, respectively. Comparison of diffusion coefficients between condition A and condition C (effect of concentration) shows a slight increase in the diffusion coefficients after reducing the concentration. However, a dramatic decrease can be observed in the diffusion coefficient of Hexabrix compared to Visipaque under

constant osmolality. The ratio of diffusion coefficients ($D_B/D_D$) for sample 1-3 was 8.6, 3.82 and 2.89, respectively.

**Table 3.3 -** Summary of diffusion coefficients for conditions A-D and samples 1-3 based on the equilibrium curves.

| Sample | $D_A$ [$\mu m^2/s$] | $D_B$ [$\mu m^2/s$] | $D_C$ [$\mu m^2/s$] | $D_D$ [$\mu m^2/s$] |
|---|---|---|---|---|
| **1** | 6.9 | 5.0 | 11.0 | 0.6 |
| **2** | 8.0 | 6.5 | 7.8 | 1.7 |
| **3** | 20.8 | 27.5 | 36.0 | 9.5 |

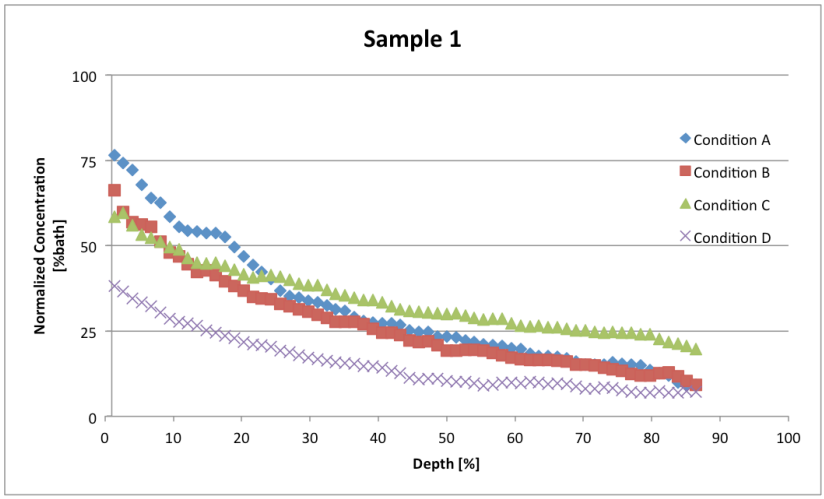


**Figure 13** – Concentration gradient curves for sample 1 at conditions A through D at time 48 hours.

# 4. Discussion

The primary aim of this thesis was to analyze the effect of contrast agent's concentration, osmolality and charge on the passive diffusion through different layers within articular cartilage. Theoretically, a solute's concentration can influence its partition coefficient [40]. However, a previous study concluded that the bath concentration of anionic contrast agents such as Hexabrix and Iodine do not have an effect on their diffusion and distribution in articular cartilage [14]. This previous study assessed the effect of concentration but in combination with charge and molecular weight which have been demonstrated to have an important effect on diffusion [14, 16, 18, 41, 42]. One of the aims of this thesis was the continuation of the previous study by using Visipaque, an uncharged contrast agent, at different concentrations to determine its effect on diffusion. By using the same neutral contrast agent at two different concentrations the effect of charge and molecular size in diffusion was eliminated. Contrary to what was hypothesized, no statistically significant differences ($P > 0.05$) were observed in the partition coefficients of conditions A and C at different time points in the equilibrium curves shown in figure 10. The effect of osmolality in diffusion was also analyzed in this thesis. The osmolalities of contrast agent solutions are often altered to match the osmolality of the synovial fluid. Ions were added to the solutions to modify their osmolality because it was hypothesized that these may have an effect on contrast agent diffusion. Previous studies have analyzed the effect of osmolality on the change of cartilage volume but not on the diffusion of the contrast agent solution [14, 43]. Using Visipaque with the same concentration at different osmolalities, the effects of charge, molecular size and concentration were eliminated to assess solely the effect of osmolality in diffusion. In figure 10, the equilibrium curves of conditions A and B were compared to assess the effect of osmolality in the diffusion of contrast agents. Contrary to what was expected, the change in osmolality did not show a statistically significant ($P > 0.05$) alteration in the diffusion of contrast agents at different time points and depths. This may be due to the fact that the amount of ions added for the adjustment of the osmolality is not enough to alter the diffusion of the solutes. The effect of charge in diffusion was also assessed during this study by comparing the diffusion of Visipaque, a neutral contrast agent, to Hexabrix, an anionic contrast agent. Both contrast agents had the same concentration and similar molecular weight to eliminate

these interactions. A previous study compared the diffusion of a neutral and a anionic contrast agent solution but at different concentrations and with different molecular weights [18]. Thus, the results although valid, may have an influence of other interactions besides charge. The equilibrium curves for conditions B and D were compared to assess the influence of charge in diffusion. As hypothesized the results were consistent with previous studies that found an inversely proportional relationship between anionic contrast agents' diffusion and spatial fixed charged density [44]. Moreover, these observations are also consistent with the expectation that anionic contrast agents reach lower equilibrium concentrations in comparison to neutral contrast agents [41]. The partition coefficients in the equilibrium curves at 48 hours of Hexabrix and Visipaque obtained in this study were 18.3 ± 9.3 % and 30.7 ± 7.4 % respectively. In a previous study, the normalized concentration of Hexabrix at 29 hours was found to be 60 ± 4 % [14] which is more than twice the value found in this study. Another study reported the normalized concentration of Gadopentetate, a neutral contrast agent, at 48 hours to be 52.7 ± 6.5 % [18]. The variation in the results may be caused by the samples used for the experiments. This study used samples extracted from equine femurs while the two other studies used samples extracted from bovine patellae. Moreover, the partition coefficient of Gadopentetate may be higher than that of Visipaque because Gadopentetate has a lower molecular weight.

The diffusion coefficients with the one dimensional finite element model developed with FEBio to fit the experimental data for all conditions in the equilibrium curves showed significant differences between conditions B and D. As expected, conditions A and B as well as A and C did not have significant differences.

Figures 11 and 12 show an important variation in the diffusion rate and partition coefficient between the different zones in cartilage. These results correlate to previous studies that determined that diffusion in the superficial zone of cartilage can be up to one hundred fold faster than in the deep zone [45-48]. The variations of diffusion rate and partition coefficients between zones in cartilage are due to the inhomogeneous property of cartilage and the interaction of the ECM and the diffusing molecules. Proteoglycan is an ECM structure that may have an effect on the diffusion of charged as well as uncharged contrast agents. A previous study showed that upon the removal of proteoglycans from cartilage, the diffusion coefficient of neutral molecules, such as dextran, increases [49]. Another study suggested that the diffusion of dextran with a molecular weight similar to that of Visipaque or Hexabrix was hindered only by

proteoglycans [47]. Nevertheless, in another study no correlation was found between the proteoglycan content in the bulk tissue and the diffusion coefficient in cartilage [30]. Due to the important property differences between cartilage's zones, zonal curves provide a more detailed and accurate information of the diffusion rate and normalized concentrations reached in each cartilage zone. The superficial zone has the highest concentration on all samples due to the high water content of cartilage in that zone. The average water content for the samples used in this study was 78%. Water acts as the medium of transport of molecules diffusing in articular cartilage, thus lower water content would decrease diffusion. The lower normalized concentrations of the middle and deep zones of cartilage are explained by the decrease of water content with depth [7]. In addition to the low water content, the deep zone has a mineralized part and small spaces that contributes to the reduction of diffusion. It was not possible to observe the influence of concentration on the equilibrium curves. However, that does not mean concentration does not have an effect on each cartilage zone. The diffusion rate of condition C was the highest in all cartilage zones. Also, condition C had a statistically significant difference from condition A in the deep zone ($P < 0.05$). These results may indicate a slight influence of concentration in diffusion. The equilibrium curves hide the effect of concentration in diffusion. This is because for the equilibrium curves, the diffusion coefficient of the superficial zone was averaged with the diffusion coefficients of the middle and deep zones that were significantly lower. Moreover, in the equilibrium curves (figure 10) it can be seen that the partition coefficients are lower than those in the superficial zone in the zonal curves (figure 12) as a consequence of the reason previously listed. Thus, the equilibrium curves shall be complemented with zonal curves to provide more accurate results. Besides concentration, a factor that may have contributed to the increased diffusivity of condition C is viscosity. For condition C, the contrast agent was diluted in PBS to reduce the concentration thereby reducing the viscosity of the solution. The reduction of viscosity may increase the partition coefficient and diffusion rate of condition C. It has been shown that diffusivity has an inverse relationship with viscosity with the fit parameter (power) that varies between -0.5 and -1 for concentrated and dilute solutions, respectively [50].

The concentration gradient shows a good correlation with the zonal curves by showing condition C having the highest normalized concentrations for the middle and deep zones. As depth progressed the normalized concentration for all conditions

decrease as was also seen on the zonal curves due to ECM interaction and water content decrease.

It is worth mentioning that a Fickean diffusion formula with a biphasic-solute model was used to calculate the diffusion coefficient of Visipaque and Hexabrix. However, the zonal curves in figure 12 show a statistically significant ($P < 0.05$) influence of concentration in the partition coefficients in the deep zone, which is not accounted for in the Fickean formula. This observation suggests that the diffusion in cartilage may be non-Fickean. For more accurate results a multiphasic model for cartilage must be developed where not only the solute, solid and water fraction is taken into account but also the uncharged particles, concentration, viscosity and other macromolecules present in cartilage can be accounted in the interaction. Nevertheless, the biphasic-solute model did not yield significant errors, especially for the overall behavior of cartilage.

We investigated the effect of osmolality, concentration and charge of the solute by means of diffusion coefficient. It has been shown that diffusivities do not undergo significant change after changing the concentration as well as the osmolality. However, from small differences between diffusivities after changing the osmolality and concentration it can be inferred that the diffusion process does not strongly follow the Fick's law. This can be explained by the fact that changes in concentration as well as the osmolality lead to enhanced solute-matrix interactions that this situation can even be accentuated once cartilage loses water as a result of exposure to high osmolality bath. Therefore, microscopic matrix shrinkage and expansion together with water content alterations lead to deviation from idea Fick's law. Nevertheless, the findings of this study do not corroborate the results of the previous study [14] that showed virtually no effect of increase/decrease of the concentration. Our study also confirmed that viscosity changes due to dilution of the bath might increase the diffusivity within the cartilage through reducing the resistance of the mass transfer in the bath-cartilage interface [50].

Influence of solute's charge is reflected by drastic decrease in diffusivity in all samples. Cartilage as a negatively charged and hydrated tissue showed noticeable resistance against penetration of negatively charged contrast agent (Hexabrix). The extremely lower values of Hexabrix diffusivity compared to those of Visipaque indicated of pronounced influence of ion-ion interaction within the cartilage's matrix.

Effects of beam hardening were found in the experiments. As the contrast agent concentration increased, so did the beam hardening. This may have had an impact on the results. Moreover, the subchondral plate was assumed to be impermeable which is not realistic as was shown in a study [46] and should be considered in future studies. Another limitation was the use of a finite bath and lack of stirring of the solution. The contrast agent molecules in a finite solution settle in the surface of cartilage, which may obstruct the diffusion of other molecules in the cartilage [45].

# 5. Conclusions

In summary, the osmolality and concentration variation in the equilibrium curves showed negligible effects on diffusion. However, in the zonal curves the concentration showed an effect on the diffusion rate of the three zones and the partition coefficient of the deep zone. This finding implies the necessity of zonal curves in combination with equilibrium curves to improve the interpretation of data. Results suggest there are important zonal differences in the composition and structure of cartilage that influence the diffusion of molecules in the tissue. Charge did have an important effect on diffusion rate, partition coefficients and diffusion coefficients as initially hypothesized. Systematic further studies are required to elucidate the contribution of macromolecules, such as proteoglycans, in diffusion. Thus, a future study could be the replication of the current study in cartilage samples that have undergone enzymatic degradation to remove proteoglycans. The samples shall be placed in an infinite bath to avoid the necessity of stirring which may have an effect on diffusion. Also, a multiphasic model for cartilage must be developed to account for the interaction of the solute, solid, water fraction, uncharged diffusing particles, macromolecules present in cartilage, viscosity and concentration of diffusing particles to calculate an accurate diffusing coefficient at each cartilage zone. Moreover, the subchondral bone should be considered as permeable.

The present results are important to enhance the current understanding of diffusion of neutral contrast agents in healthy articular cartilage. The importance of zonal curves and the influence of charge and concentration were highlighted in this study as well as the need for an enhanced multiphasic model of cartilage to improve the calculation of the diffusion coefficient in different cartilage zones.

# 6. References


1. Nordin, M. and V.H. Frankel, *Basic biomechanics of the musculoskeletal system*. 3rd ed. 2001, Philadelphia: Lippincott Williams & Wilkins. xvii, 467 p.
2. Muir, H., *Proteoglycans as organizers of the intercellular matrix.* Biochem Soc Trans, 1983. **11**(6): p. 613-622.
3. Buckwalter, J.A. and H.J. Mankin, *Articular cartilage: degeneration and osteoarthritis, repair, regeneration, and transplantation.* Instr Course Lect, 1998. **47**: p. 487-504.
4. Dougherty, G., *Image analysis in medical imaging: recent advances in selected examples.* Biomedical imaging and intervention journal, 2010. **6**(3): p. e32.
5. Buckwalter, J.A. and D.R. Lappin, *The disproportionate impact of chronic arthralgia and arthritis among women.* Clinical orthopaedics and related research, 2000. **372**: p. 159-168.
6. Bullough, P. and A. Jagannath, *The morphology of the calcification front in articular cartilage. Its significance in joint function.* Journal of Bone & Joint Surgery, British Volume, 1983. **65**(1): p. 72-78.
7. Lipshitz, H., R. Etheredge, 3rd, and M.J. Glimcher, *Changes in the hexosamine content and swelling ratio of articular cartilage as functions of depth from the surface.* J Bone Joint Surg Am, 1976. **58**(8): p. 1149-53.
8. Gu, W. and W. Lai, *A mixture theory for charged-hydrated soft tissues containing multi-electrolytes: passive transport and swelling behaviors.* Journal of biomechanical engineering, 1998. **120**(2): p. 169-180.
9. Maroudas, A., *Physicochemical properties of articular cartilage.* Adult articular cartilage, 1979. **2**: p. 215-290.
10. Garcia, A.M., et al., *Contributions of fluid convection and electrical migration to transport in cartilage: relevance to loading.* Arch Biochem Biophys, 1996. **333**(2): p. 317-25.
11. Jackson, A. and W. Gu, *Transport Properties of Cartilaginous Tissues.* Curr Rheumatol Rev, 2009. **5**(1): p. 40.
12. Berg, H.C., *Random walks in biology*. 1993: Princeton University Press.
13. Johansen-Berg, H. and T.E. Behrens, *Diffusion MRI: From quantitative measurement to in-vivo neuroanatomy*. 2009: Access Online via Elsevier.
14. Silvast, T.S., et al., *Bath Concentration of Anionic Contrast Agents Does Not Affect Their Diffusion and Distribution in Articular Cartilage In Vitro.* Cartilage, 2013. **4**(1): p. 42-51.
15. Kulmala, K., et al., *Diffusion coefficients of articular cartilage for different CT and MRI contrast agents.* Medical engineering & physics, 2010. **32**(8): p. 878-882.
16. Kokkonen, H., et al., *Detection of mechanical injury of articular cartilage using contrast enhanced computed tomography.* Osteoarthritis and Cartilage, 2011. **19**(3): p. 295-301.
17. Crank, J., *The mathematics of diffusion.* 1975.
18. Silvast, T.S., et al., *Diffusion and near-equilibrium distribution of MRI and CT contrast agents in articular cartilage.* Phys Med Biol, 2009. **54**(22): p. 6823-36.

19. Entezari, V., et al., *Effect of mechanical convection on the partitioning of an anionic iodinated contrast agent in intact patellar cartilage.* J Orthop Res, 2014. **32**(10): p. 1333-40.
20. Rieppo, J., et al., *Structure-function relationships in enzymatically modified articular cartilage.* Cells Tissues Organs, 2003. **175**(3): p. 121-132.
21. Bonassar, L.J., et al., *Inhibition of cartilage degradation and changes in physical properties induced by IL-1β and retinoic acid using matrix metalloproteinase inhibitors.* Archives of biochemistry and biophysics, 1997. **344**(2): p. 404-412.
22. Bank, R.A., et al., *Ageing and zonal variation in post-translational modification of collagen in normal human articular cartilage. The age-related increase in non-enzymatic glycation affects biomechanical properties of cartilage.* Biochem J, 1998. **330 ( Pt 1)**: p. 345-51.
23. L'Hermette, M.F., et al., *Articular cartilage, degenerative process, and repair: current progress.* Int J Sports Med, 2006. **27**(9): p. 738-44.
24. Mow, V.C., M.H. Holmes, and W.M. Lai, *Fluid transport and mechanical properties of articular cartilage: a review.* J Biomech, 1984. **17**(5): p. 377-94.
25. Lusic, H. and M.W. Grinstaff, *X-ray-computed tomography contrast agents.* Chem Rev, 2013. **113**(3): p. 1641-66.
26. Stewart, R.C., et al., *Contrast-enhanced CT with a high-affinity cationic contrast agent for imaging ex vivo bovine, intact ex vivo rabbit, and in vivo rabbit cartilage.* Radiology, 2013. **266**(1): p. 141-50.
27. Kallioniemi, A.S., et al., *Contrast agent enhanced pQCT of articular cartilage.* Physics in Medicine and Biology, 2007. **52**(4): p. 1209-1219.
28. Kokkonen, H.T., et al., *Computed tomography detects changes in contrast agent diffusion after collagen cross-linking typical to natural aging of articular cartilage.* Osteoarthritis and Cartilage, 2011. **19**(10): p. 1190-1198.
29. Maroudas, A., *Biophysical Chemistry of Cartilaginous Tissues with Special Reference to Solute and Fluid Transport.* Biorheology, 1975. **12**(3-4): p. 233-248.
30. Torzilli, P.A., T.C. Adams, and R.J. Mis, *Transient Solute Diffusion in Articular-Cartilage.* Journal of Biomechanics, 1987. **20**(2): p. 203-214.
31. Wiener, E., et al., *The Influence of Collagen Network Integrity on the Accumulation of Gadolinium-Based MR Contrast Agents in Articular Cartilage.* Rofo-Fortschritte Auf Dem Gebiet Der Rontgenstrahlen Und Der Bildgebenden Verfahren, 2011. **183**(3): p. 226-232.
32. Schneider, C.A., W.S. Rasband, and K.W. Eliceiri, *NIH Image to ImageJ: 25 years of image analysis.* Nat Methods, 2012. **9**(7): p. 671-5.
33. Doube, M., et al., *BoneJ Free and extensible bone image analysis in ImageJ.* Bone, 2010. **47**(6): p. 1076-1079.
34. Klein, S., et al., *elastix: a toolbox for intensity-based medical image registration.* IEEE Trans Med Imaging, 2010. **29**(1): p. 196-205.
35. Maes, F., et al., *Multimodality image registration by maximization of mutual information.* IEEE Trans Med Imaging, 1997. **16**(2): p. 187-98.
36. Thevenaz, P. and M. Unser, *Optimization of mutual information for multiresolution image registration.* IEEE Trans Image Process, 2000. **9**(12): p. 2083-99.

37. *MeVisLab – development environment for medical image processing and visualization. MeVis Medical Solutions AG and Fraunhofer MEVIS; Bremen, Germany: Available from:* http://www.mevislab.de/.
38. Crank, J., *XLV. A diffusion problem in which the amount of diffusing substance is finite.—IV. solutions for small values of the time.* Philosophical Magazine, 1948. **39**(292): p. 362-376.
39. Maas, S.A., et al., *FEBio: finite elements for biomechanics.* J Biomech Eng, 2012. **134**(1): p. 011005.
40. Lazzara, M.J. and W.M. Deen, *Effects of concentration on the partitioning of macromolecule mixtures in agarose gels.* J Colloid Interface Sci, 2004. **272**(2): p. 288-97.
41. Wiener, E., et al., *Contrast enhanced cartilage imaging: Comparison of ionic and non-ionic contrast agents.* Eur J Radiol, 2007. **63**(1): p. 110-9.
42. Chin, H.C., M. Moeini, and T.M. Quinn, *Solute transport across the articular surface of injured cartilage.* Arch Biochem Biophys, 2013. **535**(2): p. 241-7.
43. Wang, Q., et al., *Altered osmotic swelling behavior of proteoglycan-depleted bovine articular cartilage using high frequency ultrasound.* Phys Med Biol, 2008. **53**(10): p. 2537-52.
44. Bashir, A., et al., *Glycosaminoglycan in articular cartilage: in vivo assessment with delayed Gd(DTPA)(2-)-enhanced MR imaging.* Radiology, 1997. **205**(2): p. 551-8.
45. Maroudas, A., et al., *The permeability of articular cartilage.* J Bone Joint Surg Br, 1968. **50**(1): p. 166-77.
46. Pan, J., et al., *In situ measurement of transport between subchondral bone and articular cartilage.* J Orthop Res, 2009. **27**(10): p. 1347-52.
47. Leddy, H.A. and F. Guilak, *Site-specific molecular diffusion in articular cartilage measured using fluorescence recovery after photobleaching.* Ann Biomed Eng, 2003. **31**(7): p. 753-60.
48. Nimer, E., R. Schneiderman, and A. Maroudas, *Diffusion and partition of solutes in cartilage under static load.* Biophys Chem, 2003. **106**(2): p. 125-46.
49. Torzilli, P.A., et al., *Effect of proteoglycan removal on solute mobility in articular cartilage.* J Biomech, 1997. **30**(9): p. 895-902.
50. Pyun, C.W. and M. Fixman, *Frictional Coefficient of Polymer Molecules in Solution.* Journal of Chemical Physics, 1964. **41**(4): p. 937-&.

## Appendix A

# Registration Parameter File

```
// B-Spline transformation

//ImageTypes
(FixedInternalImagePixelType "float")
(FixedImageDimension 2)
(MovingInternalImagePixelType "float")
(MovingImageDimension 2)

//Components
(Registration "MultiResolutionRegistration")
(FixedImagePyramid "FixedRecursiveImagePyramid")
(MovingImagePyramid "MovingRecursiveImagePyramid")
(Transform "TranslationTransform")
//(Interpolator "BSplineInterpolator")
(Interpolator "LinearInterpolator")
(Optimizer "AdaptiveStochasticGradientDescent")
(ResampleInterpolator "FinalBSplineInterpolator")
(Resampler "DefaultResampler")
(Metric "AdvancedMattesMutualInformation")
(UseDirectionCosines "true")

// :::::::::::::::::::::::::::: Parameters to tune ::::::::::::::::::::::::::::::::::::

// :::: Pyramid
(NumberOfResolutions 3)
(ImagePyramidSchedule 4 4 2 2 1 1)


// :::: Optimizer - StandardGradientDescent ::::

// Maximum number of iterations
(MaximumNumberOfIterations 1024)

// :::: ImageSampler ::::

// Number of sample (2000 - 5000)
(NumberOfSpatialSamples 2048 )

// If UseRandomSampleRegion is set to "false", the sampler draws samples from
the entire image domain.
// When set to "true", the sampler randomly selects one voxel, and then selects
the remaining
// samples in a square neighbourhood (in mm) around that voxel (localized
similarity measure).
```

```
(UseRandomSampleRegion "false")
(SampleRegionSize 50.0 50.0 50.0)


// :::: Transform ::::
// Grid of control points
// This grid is defined by the spacing between the grid nodes, in voxel size
// For each resolution level you can define a different grid spacing. This is what
we call multi-grid.
// The GridSpacingSchedule defines the multiplication factors for all resolution
levels.
(FinalGridSpacingInPhysicalUnits 30.0 30.0 )
(GridSpacingSchedule 4.0 4.0  2.0 2.0  1.0 1.0 )


// ::::::::::::::::::::::::::::::::::::::::::::::::::::::::::::::::::::::::::::::


// :::: Transform ::::
// Whether transforms are combined by composition or by addition.
// In generally, Compose is the best option in most cases.
// It does not influence the results very much.
(HowToCombineTransforms "Compose")


// :::: Several ::::
(ErodeMask "false" )
(WriteTransformParametersEachIteration "false")
(WriteResultImage "true")
(CompressResultImage "false")
(WriteResultImageAfterEachResolution "false")
(ShowExactMetricValue "false")


// :::: Metric ::::
//Number of grey level bins in each resolution level:
(NumberOfHistogramBins 32 )
(FixedLimitRangeRatio 0.0)
(MovingLimitRangeRatio 0.0)
(FixedKernelBSplineOrder 1)
(MovingKernelBSplineOrder 3)
(UseFastAndLowMemoryVersion "true")


// :::: ImageSampler ::::
(ImageSampler "RandomCoordinate")
(FixedImageBSplineInterpolationOrder 1 )
(NewSamplesEveryIteration "true")
(CheckNumberOfSamples "false")
```

```
(MaximumNumberOfSamplingAttempts 10)


// :::: Optimizer - StandardGradientDescent ::::
//SP: Param_A in each resolution level. a_k = a/(A+k+1)^alpha
(SP_A 100.0 )
(ASGDParameterEstimationMethod "DisplacementDistribution")

// :::: Interpolator and Resampler ::::
//Order of B-Spline interpolation used in each resolution level:
// It may improve accuracy if you set this to 3. Never use 0.
(BSplineInterpolationOrder 1)

//Order of B-Spline interpolation used for applying the final
// deformation.
// 3 gives good accuracy.
// 1 gives worse accuracy (linear interpolation)
// 0 gives worst accuracy, but may be appropriate for
// binary images; this would be equivalent to nearest neighbor
// interpolation.
(FinalBSplineInterpolationOrder 3)

//Default pixel value for pixels that come from outside the picture:
(DefaultPixelValue 0)

(MaximumStepLength 0.7)
```

## Appendix B

# Elastix Usage Example

Elastix is a command-line program with no graphical user interface. The command line arguments can be generated by calling:

```
elastix - - help
```

To run a registration, the following basic command can be used:

```
elastix –f dir.ext –m dir.ext –out dir –p par.txt
```

In this command, after `–f` and `–m` the directory where the fixed $I_F$ and the moving image are located is listed respectively. Also, `ext` is the supported extension for the image file formats. The output information is written in the specified directory after `–out`. The parameter file lists the components selected and their corresponding parameters. An example of a parameter file can be seen in Appendix A.

# Appendix C

## MeVisLab Network

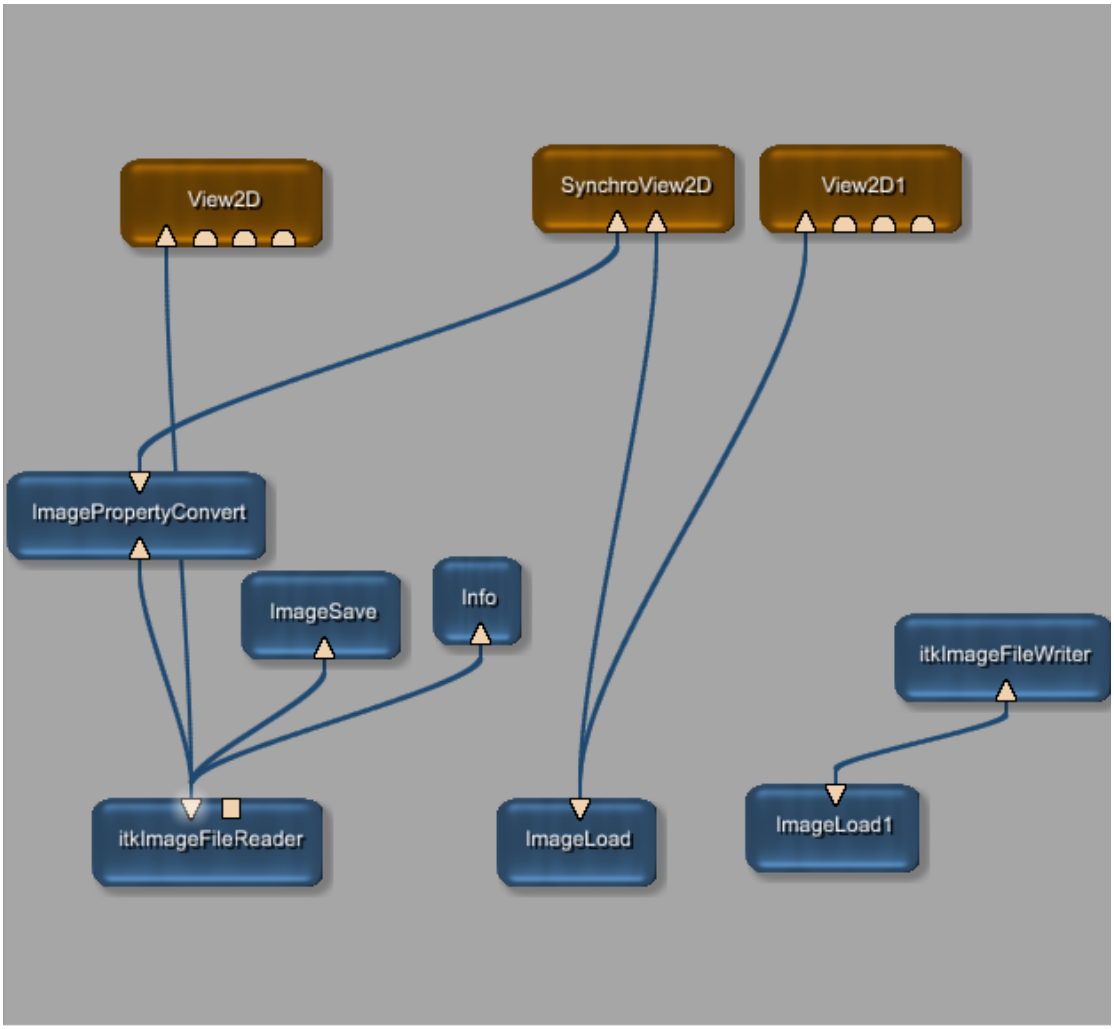


**Figure 14 -** Network generated to compare registered images to fixed images.

Figure 14 shows the network created to simultaneously visualize the results of registration and compare them to the fixed image. Moving and fixed images were transformed from .tiff extension to .mhd extension using the itkImageFileWriter module and loaded into MeVislab using the ImageLoad1 module. The .mhd format was needed for registration with elastix software. After obtaining the registered images with elastix, the fixed image was loaded into the Image Load module. The registered image was loaded into the itkImageFileReader. Using the module SynchroView2D allowed the simultaneous visualization of the registered and fixed images evaluate the accuracy of the registration process.